14th International Symposium on Turbulence and Shear Flow Phenomena (TSFP14)
Heidelberg, Germany, July 28-31, 2026

REDUCTION OF PRESSURE FLUCTUATIONS IN INCOMPRESSIBLE CAVITY FLOWS BY MULTIPLE SLOT JETS

Seungho Yoo
Department of Mechanical Engineering
UNIST
50 UNIST-gil, Eonyang-eup, Ulsan, 44919, Korea
seungho@unist.ac.kr

Jae Hwa Lee
Department of Mechanical Engineering
UNIST
50 UNIST-gil, Eonyang-eup, Ulsan, 44919, Korea
jhlee06@unist.ac.kr

ABSTRACT

Large-eddy simulations are performed to investigate the effects of three-dimensional (3-D) wall-normal steady blowing on pressure fluctuations in an incompressible turbulent cavity flow. The cavity has a length-to-depth ratio (L/D) of 2 and the Reynolds number based on the cavity depth (Re_D) is 12,000. The steady blowing is applied upstream of the cavity leading edge through multiple slots while varying the number of slots (N_{slot}) and the spatial duty cycle (l/λ), where l is the spanwise length of each slot and λ is the center-to-center spacing between adjacent slots. The control performance is then evaluated by the surface-integrated root-mean-square of the pressure fluctuations along the cavity wall, and the most effective and degraded control cases are identified when N_{slot} = 32 and 4 under a fixed l/λ = 0.25, respectively. When the slots are dense (i.e., N_{slot} = 32), the blowing jets disrupt the spanwise coherence of large-scale vortical structures in the shear layer by generating 3-D disturbances across the span. The weakened impingement of the vortical structures on the cavity aft wall reduces the pressure fluctuations by up to 15.5% compared to the uncontrolled baseline case, outperforming the two-dimensional steady blowing control (7.59%). In contrast, when the slots are excessively wide (i.e., N_{slot} = 4), 3-D disturbances are induced near the slot locations, resulting in a wavy shear layer with intensified large-scale vortical structures. The associated strong impingement of the shear layer promotes the generation of small-scale vortices within the cavity, amplifying the pressure fluctuations.

INTRODUCTION

Turbulent flow over an open cavity is observed in a wide range of engineering applications, such as scramjet combustors, internal bomb bays, landing gear wells in aircraft, sunroofs in automobiles, panel gaps on trains and moonpool in maritime application. Despite its geometric simplicity, turbulent cavity flows exhibit complex behavior, often resulting in self-sustained oscillations. Such oscillations are known to produce strong pressure fluctuations and energy spectral peaks, causing structural damage, vibration, and intense acoustic noise, especially near the trailing edge of the cavity (Rockwell and Naudascher 1978).

In compressible cavity flows, small disturbances generated by Kelvin–Helmholtz instabilities in a separated shear layer grow as they convect downstream, impinge upon the trailing edge, and produce upstream-propagating acoustic waves. The generated acoustic waves amplify the shear layer instabilities near the leading edge, forming an acoustic feedback loop that sustains oscillations. In contrast, incompressible cavity flows lack a dominant acoustic feedback loop due to the absence of significant acoustic wave propagation. Instead, self-sustained oscillations arise from an interaction between large-scale vortical structures in the shear layer and a recirculating flow. An experimental study by Lin and Rockwell (2001) showed that the impingement of large-scale vortical structure on the aft wall generates small-scale vortices, which are periodically entrained into the recirculation zone within the cavity. The generated small-scale vortices propagate upstream and re-enter the shear layer, thereby amplifying its instabilities.

Various passive and active control methods have been applied to suppress self-sustained oscillations in turbulent cavity flows (Lawson and Barakos 2011). In particular, active methods offer greater adaptability by directly manipulating the shear layer through actuators such as steady or pulsed blowing jets (Lamp and Chokani 1997). In compressible cavity flows, Li et al. (2013) conducted large-eddy simulations (LES) with a two-dimensional (2-D) single-slot configuration to examine the effect of wall-normal steady blowing on pressure fluctuations. They showed that lifting the shear layer away from the trailing edge weakens the impingement of vortices on the aft wall, resulting in a significant reduction of pressure fluctuations over the entire cavity walls. More recently, Zhang et al. (2019) performed both experimental and LES studies using multiple slots (i.e., three-dimensional (3-D) steady blowing). They reported that counter-rotating vortices disrupt the spanwise coherence of large-scale vortical structures and thus suppresses the acoustic feedback loop with superior performance compared to the 2-D steady blowing.

In incompressible cavity flows, however, investigations of the influence of the steady blowing jet on the self-sustained oscillations have been carried out only using 2-D steady blowing. Choi and Lee (2023) performed LES with 2-D steady blowing and showed that the wall-normal steady blowing can reduce pressure fluctuations. They also reported the existence of an optimal blowing jet intensity beyond which the control performance deteriorates due to intensified internal cavity flow. Although their findings provide important insight into the feasibility of steady blowing in incompressible cavity flows, the scope has been confined to 2-D slot configuration. Consequently, the influence of 3-D slot blowing on the suppression of pressure fluctuations remains largely unexplored. In the present study, we performed LES of incompressible cavity flows to examine the effects of 3-D slot jets on hydrodynamic feedback loops.

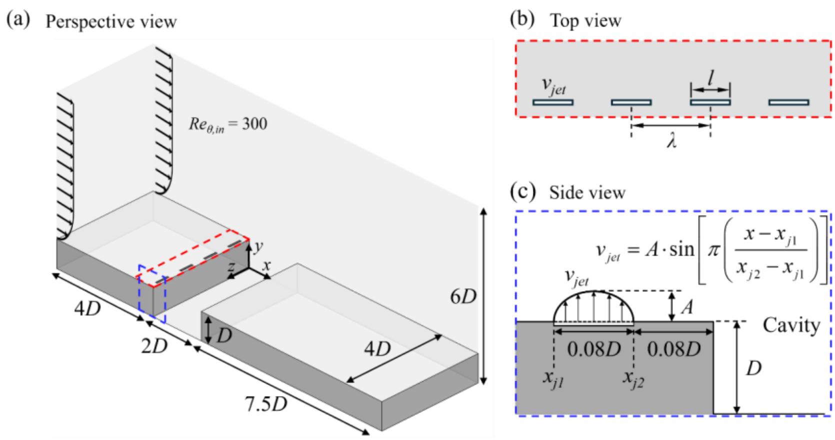

Figure 1. Schematic of (a) the computational domain for a turbulent cavity flow (perspective view), (b) the multiple slot configuration (top view) and (c) the sinusoidal velocity profile (side view) of the wall-normal steady blowing (not to scale). In (b), the spanwise length of each slot and the center-to-center spacings are represented by l and λ, respectively, and the gap between the slots is λ-l. Here, as a representative, a slot array with $N_{slot} = 4$ and $l/\lambda = 0.50$ is plotted. In (c), wall-normal steady blowing with a sinusoidal velocity profile (v_{jet}) imposed through limited transverse slots in an upstream region of the leading edge is shown. The blowing amplitude is represented by A and streamwise edge positions are denoted by x_{j1} and x_{j2}, respectively.

COMPUTATIONAL DETAILS

The non-dimensional governing equations for LES of incompressible turbulent flows, consisting of the spatially filtered continuity and Navier-Stokes equations, are given as follows:

$$\frac{\partial \bar{u}_i}{\partial x_i} = 0,\quad \frac{\partial \bar{u}_i}{\partial t} + \frac{\partial \bar{u}_i \bar{u}_j}{\partial x_j} = -\frac{\partial \bar{p}}{\partial x_i} + \frac{1}{Re_D}\frac{\partial^2 \bar{u}_i}{\partial x_j^2} - \frac{\partial \tau_{ij}}{\partial x_j}, \quad (1)$$

$$\tau_{ij} = \overline{u_i u_j} - \bar{u}_i \bar{u}_j, \quad (2)$$

where x_i denotes the Cartesian coordinates, $\bar{u}_i$ and $\bar{p}$ are the spatially filtered velocity and pressure and u_i is the instantaneous velocity component in the i-direction (i = 1-3). The overbar indicates a quantity obtained using an implicit top-hat filter. The notation adopted is such that x (= x_1), y (= x_2), and z (= x_3) represent the streamwise, wall-normal and spanwise coordinates, respectively, and that $\bar{u}$ (= $\bar{u}_1$), $\bar{v}$ (= $\bar{u}_2$), and $\bar{w}$ (= $\bar{u}_3$) denote the corresponding velocity components. All variables are normalized by the free-stream velocity (U_∞) and the cavity depth (D). The Reynolds number is defined as $Re_D = U_\infty D/\nu$, where ν is the kinematic viscosity. The sub-grid scale (SGS) stress tensor (τ_{ij}) is calculated based on the dynamic Smagorinsky model proposed by Germano et al. (1991). The governing equations are integrated in time using a fully implicit fractional-step method that is coupled with the implicit velocity decoupling procedure proposed by Kim et al. (2002). In the present study, several averaging procedures are employed to obtain converged turbulent statistics. Angle brackets with subscripts ϕ, t and/or z indicate a phase-, temporal- and/or spanwise-averaging, respectively. Further numerical details can be found in Lee et al. (2010).

A schematic of the computational domain for a turbulent cavity flow is shown in figure 1(a). These domain dimensions are chosen based on the two-point correlations of the velocity fluctuations decaying to zero (Lee et al. 2010). The cavity considered in the present study has L/D = 2 and the Reynolds number is Re_D = 12,000. Under this configuration, Lee et al. (2010) successfully confirmed the presence of self-sustained oscillations in the incompressible turbulent cavity flow.

Table 1. Numerical details for LES of turbulent cavity flows

D/θ_{in}	N_x, N_y, N_z	Δx_{min}^+, Δx_{max}^+	Δy_{max}^+	Δz^+
40	897, 169, 257	1.4, 40	0.56	10

Realistic inlet velocity profiles are generated at $Re_{\theta,in}$ (= $U_\infty \theta_{in}/\nu$) = 300 by an auxiliary simulation based on the recycling method of Lund et al. (1998). A convective outflow condition is applied at the domain exit. No-slip boundary conditions are imposed on the walls, while a Neumann boundary condition is applied at the top boundary. Periodic boundary conditions are applied in the spanwise direction. Non-uniform grids are used in both the streamwise and wall-normal directions, while a uniform grid is used in the spanwise direction. Additional numerical details for the LES are summarized in Table 1. The time step is fixed at a small value of $\Delta t = 0.001875D/U_\infty$ due to the explicit characteristics of the dynamic Smagorinsky model. Although not shown here, the validation of the present numerical simulations is conducted by an additional LES of turbulent cavity flow with L/D = 1 and compared with the experimental data by Kang et al. (2008) when Re_D = 11,650 ($Re_{\theta,in}$ = 830). In the present study, 3-D wall-normal steady blowing is applied through multiple slots that are uniformly distributed in the spanwise direction. In figure 1(b), the spanwise length of each slot and the center-to-center spacing between adjacent slots are denoted by l and λ, respectively, and thus the gap between the slots is λ-l. As shown in figure 1(c), each slot is located 0.08D upstream of the leading edge of the cavity and has a streamwise extent of 0.08D, following the configuration used by Li et al. (2013) for compressible cavity flows. To prevent the velocity discontinuities near the slot edges, the jet velocity profile follows a sinusoidal function. The blowing amplitude (A) is determined from the non-dimensional momentum coefficient (C_μ) through the slots following Ukeiley et al. (2008), where C_μ is fixed at 0.015, corresponding to the optimal value reported for 2-D steady blowing under identical flow conditions. The control performance is evaluated using the reduction rate of the surface-integrated root-mean-square (rms) of the filtered pressure fluctuations along the entire cavity wall, as suggested by Lusk et al. (2012):

$$\bar{p}'_{rms} = \int_{\tilde{\Omega}} \frac{\bar{p}'_{rms}}{0.5\rho_\infty U_\infty^2} d\tilde{\Omega}, \tag{3}$$

$$\%\bar{p}'_{rms,reduction} = \frac{\bar{p}'_{rms,controlled} - \bar{p}'_{rms,baseline}}{\bar{p}'_{rms,baseline}} \times 100\%, \tag{4}$$

where $\tilde{\Omega}$ denotes the cavity wall surface. Equation (4) quantifies the change in pressure fluctuations relative to the baseline (i.e., an uncontrolled cavity flow): a negative value indicates the reduction. In this study, various slot configurations are examined by varying the number of slots (N_{slot} = 4, 8, 16, 32 and 64) and the normalized spanwise extent of each slot (l/λ = 0.25, 0.5 and 0.75) to investigate modifications to the hydrodynamic feedback loop.

RESULTS AND DISCUSSION

Uncontrolled turbulent cavity flow

Before examining in detail how the wall-normal steady blowing via multiple slot jets affects the suppression of pressure fluctuations induced by self-sustained oscillations on the cavity walls, we first identify the presence of self-sustained oscillations in an uncontrolled baseline cavity flow. Figure 2(a) visualizes the iso-surface of instantaneous vortical structures in a turbulent cavity flow, identified using the swirling strength (λ_{ci}) colored by the filtered pressure fluctuation (Zhou et al. 1999). In the figure, the vortical structures with negative pressure fluctuations (blue color) responsible for the self-sustained oscillations are observed in the shear layer, and these vortical structures convect downstream with varying length scales. To quantify the length scales for the vortical structures, the two-point spatial correlation coefficients of the filtered pressure fluctuations ($R_{\bar{p}'\bar{p}'}$) are calculated as :

$$R_{\bar{p}'\bar{p}'}\left(x,y;x_{ref},y_{ref}\right) = \frac{\left\langle \bar{p}'\left(x_{ref},y_{ref},z,t\right)\bar{p}'\left(x,y,z+r_z,t\right)\right\rangle_{tz}}{\bar{p}'_{rms}\left(x_{ref},y_{ref}\right)\bar{p}'_{rms}\left(x,y\right)}, \tag{5}$$

where x_{ref} and y_{ref} are the reference locations in the streamwise and wall-normal directions, respectively. Figures 2(b-e) show the contours of the two-point correlation coefficients of the filtered pressure fluctuations on the xy-plane (at r_z/D = 0.0) obtained at four different streamwise locations (i.e., x_{ref}/D = 0.5, 1.0, 1.5 and 1.95). In the figure, the solid and dotted lines represent positive and negative correlation coefficients, respectively. The wall-normal reference location is y_{ref}/D = 1.0. The streamwise length scale of the vortical structures is estimated based on a region for which $R_{\bar{p}'\bar{p}'} \geq 0.2$, according to a previous study by Choi and Lee (2023). As the vortical structures move downstream, the streamwise length scale of the structures increases from 0.2D at x_{ref}/D = 0.5 to 0.4D at x_{ref}/D = 1.5, consistent with earlier observations (Lee et al. 2010) This indicates that small-scale vortical structures grow into large-scale vortical structures as they move downstream. However, when the vortical structures approach the aft wall (figure 2e), the streamwise length scale decreases due to the clipping of the vortical structures by impingement on the aft wall (Rockwell and Knisely 1979). This impingement of the vortical structures is known to contribute to the generation of the hydrodynamic feedback loop within the cavity, resulting in self-sustained oscillations with strong pressure fluctuations (Pereira and Sousa 1995).

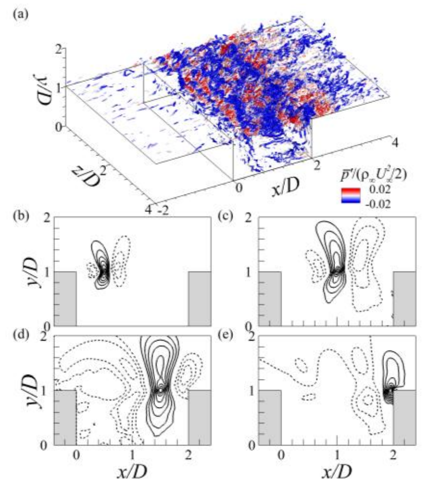

Figure 2. (a) Instantaneous vortical structures visualized by an iso-surface of swirling strength (λ_{ci}) colored by the filtered pressure fluctuations ($\bar{p}'$). The iso-surface is 4% of the maximum λ_{ci} to depict the vortical structures. (b-e) Contours of the two-point correlation coefficients ($R_{\bar{p}'\bar{p}'}$) at four different streamwise locations along the cavity lip line (y_{ref}/D = 1.0) on the xy-plane (at r_z/D = 0.0): (b) x_{ref}/D = 0.5, (c) 1.0, (d) 1.5 and (e) 1.95. The contour levels are varied from -0.3 to 0.9 with an interval of 0.1. Dashed contour lines indicate negative values.

Table 2. Control performance of the wall-normal blowing for various slot configurations.

Case name	N_{slot}	l/λ	$\%\bar{p}'_{rms,reduction}$
Baseline	-	-	-
2-D control	1	1	−7.59%
***N*04*S*25**	4		**+61.3%**
*N*08*S*25	8		+15.5%
*N*16*S*25	16	0.25	−9.96%
***N*32*S*25**	32		**−15.5%**
*N*64*S*25	64		−15.5%
*N*04*S*50	4		+28.1%
*N*08*S*50	8		+19.8%
*N*16*S*50	16	0.50	+1.89%
*N*32*S*50	32		−12.2%
*N*64*S*50	64		−10.9%
*N*04*S*75	4		+7.12%
*N*08*S*75	8		+6.41%
*N*16*S*75	16	0.75	−14.4%
*N*32*S*75	32		−4.74%
*N*64*S*75	64		−9.96%

Active flow control using multiple slot jets

To evaluate the effect of 3-D steady blowing on the suppression of the pressure fluctuations, the reduction rate of the

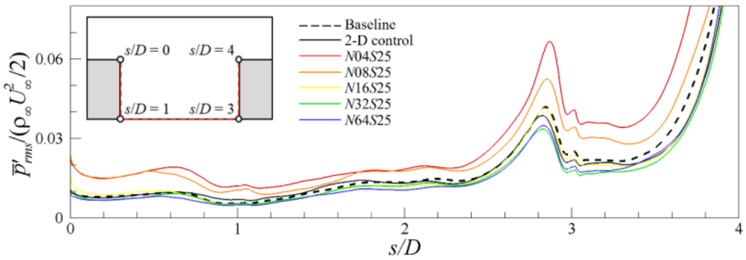

Figure 3. Distributions of the rms of the pressure fluctuation ($\overline{p}'_{rms}$) along the cavity wall along the coordinate s/D (see the inset).

pressure fluctuations within the cavity are summarized in Table 2 for various slot configurations when the number of slots (N_{slot}) and spatial duty cycles (l/λ) vary. The case name in Table 2 is defined in terms of the two varying parameters (N_{slot} and l/λ) determining each slot configuration. Here, N_{slot} is abbreviated as N and the spatial duty cycle l/λ is denoted by S, where its value is expressed in percent. For example, $N04S25$ indicates a slot configuration with $N_{slot} = 4$ and $l/\lambda = 0.25$. In the table, it is clear that the effectiveness of the control strongly depends on both the number of slots and the spatial duty cycle. When the spatial duty cycle l/λ is fixed, an increase in N_{slot} generally reduces the pressure fluctuations. Furthermore, when N_{slot} is small (e.g., $N_{slot} = 4$), increasing the spatial duty cycle (l/λ) leads to a reduction in the pressure fluctuations. The most important finding from the table is that the 3-D control case at an optimal slot configuration ($N32S25$) achieves a maximum reduction of 15.5% (see bold number) relative to the baseline. This substantially exceeds the 7.59% reduction achieved with the 2-D control case at its optimal momentum coefficient (C_μ). This result is consistent with the findings of Zhang et al. (2019) for compressible cavity flows, suggesting that the 3-D control more effectively suppresses the pressure fluctuations associated with the hydrodynamic feedback loop in incompressible cavity flows.

To further examine how the pressure fluctuations are modified along the cavity wall for various slot configurations, figure 3 presents the variation of $\overline{p}'_{rms}$ along the cavity wall for $N_{slot} = 4$, 8, 16, 32 and 64 at a fixed spatial duty cycle of $l/\lambda = 0.25$. Here, a non-dimensional coordinate (s/D) is newly introduced along the cavity wall, which traces the internal cavity wall from the leading edge, along the bottom wall, and up to the trailing edge (see the inset in figure 3). For 2-D control (black solid line), a clear reduction is observed on the aft wall ($2.8 < s/D < 4.0$) compared to the baseline (bold dashed line), although a relatively localized increase is found in the upstream region ($0.6 < s/D < 1.8$). Choi and Lee (2023) showed that the reduction of $\overline{p}'_{rms}$ along the downstream wall ($2.8 < s/D < 4.0$) results from the lifted shear layer, which mitigates the impingement of large-scale vortical structures near the trailing edge. In addition, they reported that the increase in $\overline{p}'_{rms}$ observed in the upstream region ($0.6 < s/D < 1.8$) is due to the intensified recirculating flow within the cavity. On the other hand, for the 3-D slot configurations with large N_{slot} (=32 and 64), the reduction relative to the baseline is observed along the entire cavity wall. This demonstrates that the 3-D slot configurations achieve a more effective suppression along the entire cavity wall than the 2-D control by overcoming its inherent limitation in the upstream region and by further reducing $\overline{p}'_{rms}$ in the downstream region. Contrary to the observation for the large N_{slot}, when N_{slot} is small (=4 and 8), $\overline{p}'_{rms}$ is generally higher than the baseline over most of the cavity walls, indicating the need to optimize the control performance with respect to N_{slot}.

Suppression of large-scale vortical structures

To elucidate how and why the best and worst control performances are observed for the 3-D control cases depending on the parameters, two representative 3-D steady blowing cases are considered: the coarse slot configuration ($N04S25$), which exhibits the most degraded control performance and the dense slot configuration ($N32S25$), which provides the most effective suppression of self-sustained oscillations (see bold entries in Table 2). Figure 4 visualizes an iso-surface of instantaneous vortical structures to examine the effects of the steady blowing on the vortical structures in the shear layer. The instantaneous vortical structures in figure 4(a) are extracted using the swirling strength ($\lambda_{ci}D/U_\infty$=5) colored by the filtered pressure fluctuations, while the iso-surface of the negative filtered pressure fluctuations in figure 4(b) highlights the regions associated with the cores of vortical structures. In addition, because it has been reported that the development of vortical structures within the shear layer is closely associated with the elevated values of the rms of the filtered wall-normal velocity fluctuations ($\overline{v}'_{rms}$) (Haigermoser et al. 2008), the contours of $\overline{v}'_{rms}$ on the yz-plane are plotted in figure 5 at three different streamwise locations (x/D = 0.5, 1.0 and 1.5) to identify the modification of the large-scale vortical structures in the shear layer. For the baseline (see figures 4a-i and 4b-i), the shear layer develops into spanwise-aligned large-scale vortical structures through spanwise-coherent roll-up, which are characterized by elongated regions of negative filtered pressure fluctuations. This organization of the large-scale vortical structures creates a prominent region of high $\overline{v}'_{rms}$ along the cavity lip line (see the white dashed line in figure 5a) as the structures move along the downstream direction, $\overline{v}'_{rms}$ with little variation in the spanwise direction. Similar to the baseline case, the spanwise-aligned large-scale vortical structures are found for the 2-D control case in figures 4(a-ii) and (b-ii), indicating that the 2-D steady blowing has little influence on the large-scale vortical structures. However, as shown in figure 5(b), the strong $\overline{v}'_{rms}$ region is shifted to a higher wall-normal position compared to the baseline, consistent with the lifted shear layer reported by Choi and Lee (2023).

On the other hand, for $N04S25$ in figures 4(a-iii) and (b-iii), the clustered iso-surface of λ_{ci} becomes more intensified over the entire shear layer, accompanied by locally strong regions of the negative pressure fluctuations. The amplification of the vortical activity within the shear layer for $N04S25$ can be confirmed via the corresponding $\overline{v}'_{rms}$ distribution in figure 5(c). In addition to an overall increase in strength of the large-scale structures, the distribution exhibits a clear spanwise variation aligned with the slot locations, reflecting the development of a wavy shear layer along the streamwise direction. The spanwise variations in the wall-normal position of the shear layer subsequently lead to non-uniform impinging behavior shown later. For *N*32*S*25 with the dense slot configuration in figures 4(a-iv) and (b-iv), the elongated regions of the negative pressure fluctuations lose their spanwise coherence in the shear layer. As a result, the magnitude of $\overline{v}'_{rms}$ in figure 5(d) is significantly reduced compared to the other cases without a clear spanwise modulation.

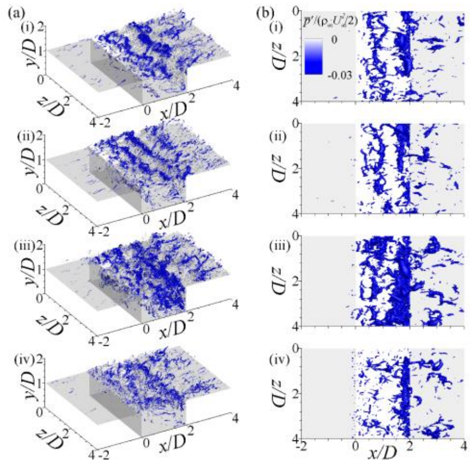

Figure 4. (a) Iso-surface of the instantaneous vortical structure visualized by λ_{ci} ($\lambda_{ci}U_\infty/D$ = 5) on the perspective view and (b) iso-surface of the filtered pressure fluctuations on the top view: (i) baseline, (ii) 2-D control, (iii) *N*04*S*25 and (iv) *N*32*S*25.

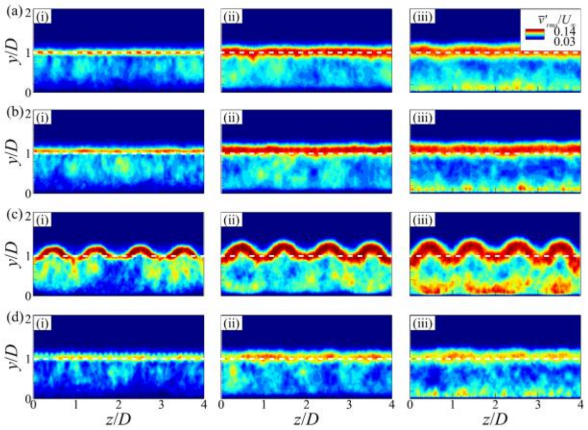

Figure 5. Contours of the rms of the wall-normal velocity fluctuations on the *yz*-plane for (a) baseline, (b) 2-D control, (c) *N*04*S*25 and (d) *N*32*S*25: (i) *x*/*D* = 0.5, (ii) *x*/*D* = 1.0 and (iii) *x*/*D* = 1.5. The cavity lip line (*y*/*D* = 1.0) is represented with the white dashed line.

Stabilization of the internal cavity flow

We have shown that the 3-D steady blowing via the multiple slot jets alters the spanwise organization of the large-scale vortical structures responsible for self-sustained oscillations associated with the hydrodynamic feedback loop. However, it remains unclear how modified large-scale vortical structures by the different slot configurations interact with the recirculating flow, leading to the contrasting control performance observed for *N*04*S*25 and *N*32*S*25. To address this issue, we examine the influence of the slot configurations on the recirculating flow within the cavity. Because it is well known that additional mass injection (i.e., wall-normal blowing) upstream of the cavity lifts the shear layer, thereby mitigating the impingement of vortical structures on the aft wall (Li et al. 2013), the effects of wall-normal blowing on the modification of the shear layer near the trailing edge and its influence on the internal cavity flow are investigated.

Figures 6(a, b) show the iso-surface of the time-averaged streamwise velocity at for *N*04*S*25 and *N*32*S*25 to highlight the spatial modification of the shear layer. In addition, the streamwise variation of the wall-normal position of the shear layer (y_{SL}/D) for each case is plotted in figures 6(c) and (d) together with those of the baseline and 2-D control cases. Because the shear layer in the 3-D control case exhibits a clear spanwise variation, two representative spanwise locations, (I) and (II), are defined (see the inset in figure 6c). Here, (I) corresponds to the midpoint between adjacent slots and (II) depicts each slot center. As expected, the shear layer for the 2-D control case (black solid line) in figure 6(c) is lifted compared to the baseline (black dashed line) due to the steady blowing. For *N*04*S*25 (red line) in figure 6(c), the shear layer at location (II) is lifted higher than that for the 2-D control, whereas at location (I) it remains lower than that for the baseline. For *N*32*S*25 (figure 6d), the shear layer at location (II) is lifted near the leading edge, whereas it is not at location (I). As the shear layer for *N*32*S*25 travels along the downstream direction, the dependence on the spanwise location disappears and the lifting of the shear layer is not significant compared to the 2-D control.

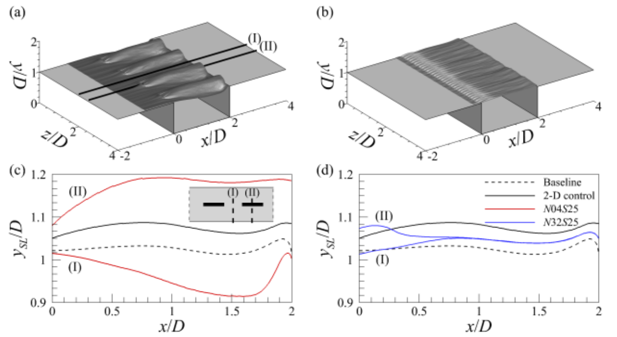

Figure 6. Iso-surface of the time-averaged streamwise velocity ($\langle \overline{u} \rangle_t = 0.5U_\infty$) for (a) *N*04*S*25 and (b) *N*32*S*25

Figures 7(a-d) show the time evolution of the instantaneous spanwise vorticity contours with swirling strength ($\lambda_{ci}\omega_z/|\omega_z|$ = 1.0) on the *xy*-plane to elucidate the influence of the wall-normal steady blowing on the self-sustained oscillations. The mean streamwise velocity profiles are provided in figure 8 to supplement the analysis. Consistent with previous observation for incompressible cavity flows (Lin and Rockwell 2001), the primary vortex (figure 7a) established by the shear layer entrainment for the baseline case interacts with the no-slip cavity aft wall, thereby generating small-scale positive spanwise vortices (red color) along the cavity aft wall in figure 7(a-i). These small-scale vortices propagate toward the upstream shear layer near the leading edge of the cavity with time (figures. 7a-ii-iv) and contribute to an increase in the flow instability. For the 2-D control case (figure 7b), an intensified reverse flow observed in figure 8 promotes the upstream propagation of the small-scale vortices generated near the aft wall, increasing $\overline{p}'_{rms}$ in the upstream region of the cavity (figure 3). Although the magnitude of the reverse flow also increases slightly in the downstream region, the lifted shear layer weakens the impingement of the large-scale vortical structures on the aft wall, thereby reducing $\overline{p}'_{rms}$ in the downstream region of the cavity. For *N*04*S*25, the magnitude of the reverse flow is substantially enhanced throughout the cavity (see the red lines in figure 8) due to the intense impingement of the shear layer at location (I) (figure 6c). As a result, highly intensified small-scale vortices (figure 7c) are generated near the aft wall, contributing to the highest $\overline{p}'_{rms}$ along the cavity wall. In contrast, although the magnitude of the reverse flow for *N*32*S*25 increases inside the cavity compared to the baseline (blue lines in figure 8) due to the slightly lifted shear layer (figure 6d), the weakened large-scale vortical structures generate fewer small-scale vortices with relatively weak strength near the aft cavity wall. Thus, the reduction in the number of small-scale vortices attenuates on the aft wall and weakens their upstream influence, resulting in an overall mitigation of $\overline{p}'_{rms}$ along the cavity wall in figure 3.

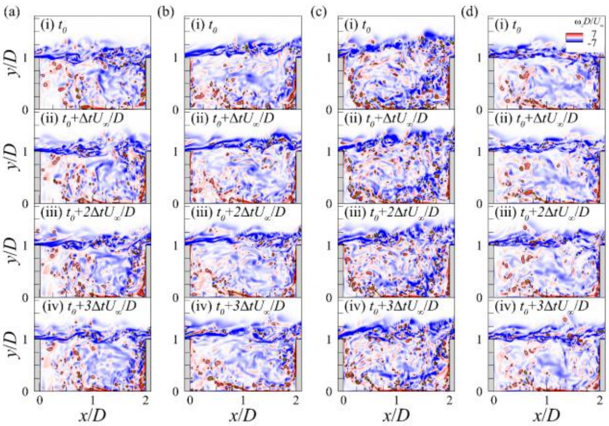

Figure 7. Temporal evolution of the vortical structures within the cavity visualized by contours of instantaneous spanwise vorticity ($\omega_z D/U_\infty$) for (a) baseline, (b) 2-D control, (c) *N*04*S*25 and (d) *N*32*S*25. Snapshots are shown at four time instances with a constant time interval ($\Delta t U_\infty/D$ = 0.375): (i) t_0, (ii) $t_0 + \Delta t U_\infty/D$, (iii) $t_0 + 2\Delta t U_\infty/D$ and (iv) $t_0 + 3\Delta t U_\infty/D$.

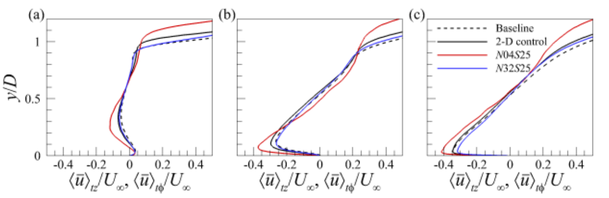

Figure 8. Profiles of the time- and spanwise- (or phase-) averaged streamwise velocity for the baseline and 2-D control ($\langle \overline{u} \rangle_{tz}/U_\infty$), *N*04*S*25 and *N*32*S*25 ($\langle \overline{u} \rangle_{t\phi}/U_\infty$) at (a) x/D = 0.5, (b) x/D = 1.0, and (c) x/D = 1.5 at location (II).

REFERENCES

Choi, J. N. and Lee, J. H. 2023, "Active control of pressure fluctuations in an incompressible turbulent cavity flow," *Aerosp. Sci. Technol.*, 141, 108512.

Germano, M., Piomelli, U., Moin, P. and Cabot, W. H. 1991, "A dynamic subgrid-scale eddy viscosity model," *Phys. Fluids A*, 3, 1760–1765.

Haigermoser, C., Vesely, L., Novara, M. and Onorato, M. 2008, "A time-resolved particle image velocimetry investigation of a cavity flow with a thick incoming turbulent boundary layer," *Phys. Fluids*, 20.

Kang, W., Lee, S. B. and Sung, H. J. 2008, "Self-sustained oscillations of turbulent flows over an open cavity," *Exp. Fluids*, 45, 693–702.

Kim, K., Baek, S. J. and Sung, H. J. 2002, "An implicit velocity decoupling procedure for the incompressible Navier–Stokes equations," *Int. J. Numer. Methods Fluids*, 38, 125–138.

Lamp, A. M. and Chokani, N. 1997, "Computation of cavity flows with suppression using jet blowing," *J. Aircr.*, 34, 545–551.

Lawson, S. and Barakos, G. N. 2011, "Review of numerical simulations for high-speed, turbulent cavity flows," *Prog. Aerosp. Sci.*, 47, 186–216.

Lee, S. B., Seena, A. and Sung, H. J. 2010, "Self-sustained oscillations of turbulent flow in an open cavity," *J. Aircr.*, 47, 820–834.

Li, W., Nonomura, T. and Fujii, K. 2013, "Mechanism of controlling supersonic cavity oscillations using upstream mass injection," *Phys. Fluids*, 25.

Lin, J.-C. and Rockwell, D. 2001, "Organized oscillations of initially turbulent flow past a cavity," *AIAA J.*, 39, 1139–1151.

Lund, T. S., Wu, X. and Squires, K. D. 1998, "Generation of turbulent inflow data for spatially-developing boundary layer simulations," *J. Comput. Phys.*, 140, 233–258.

Lusk, T., Cattafesta, L. and Ukeiley, L. 2012, "Leading edge slot blowing on an open cavity in supersonic flow," *Exp. Fluids*, 53, 187–199.

Pereira, J. C. F. and Sousa, J. M. M. 1995, "Experimental and Numerical Investigation of Flow Oscillations in a Rectangular Cavity," *J. Fluids Eng.*, 117, 68–74.

Rockwell, D. and Knisely, C. 1979, "The organized nature of flow impingement upon a corner," *J. Fluid Mech.*, 93, 413–432.

Rockwell, D. and Naudascher, E. 1978, "Self-sustaining oscillations of flow past cavities," *J. Fluids Eng.*, 100, 152–165.

Ukeiley, L., Sheehan, M., Coiffet, F., Alvi, F., Arunajatesan, S. and Jansen, B. 2008, "Control of pressure loads in geometrically complex cavities," *J. Aircr.*, 45, 1014–1024.

Zhang, Y., Sun, Y., Arora, N., Cattafesta Iii, L. N., Taira, K. and Ukeiley, L. S. 2019, "Suppression of cavity flow oscillations via three-dimensional steady blowing," *AIAA J.*, 57, 90–105.

Zhou, J., Adrian, R. J., Balachandar, S. and Kendall, T. 1999, "Mechanisms for generating coherent packets of hairpin vortices in channel flow," *J. Fluid Mech.*, 387, 353–396.